Korean J. Chem. Eng., 32(4), 723-730 (2015)
DOI: 10.1007/s11814-014-0273-2

pISSN: 0256-1115
eISSN: 1975-7220

Preparation of activated carbon from fly ash and its application for CO_2 capture

Yahia Abobakor Alhamed*,,†, Sami Ullah Rather*,**,†, Ahmad Hasan El-Shazly*,**, Sharif Fakhruz Zaman*,**, Mohammad Abdulrhaman Daous*,**, and Abdulrahim Ahmad Al-Zahrani*,****

*Chemical and Materials Engineering Department, King Abdulaziz University, P. O. Box 80204, Jeddah 21589, Saudi Arabia
**Center of Excellence in Environmental Studies, King Abdulaziz University, P.O. Box 80216, Jeddah 21589, Saudi Arabia
(*Received 5 May 2014 • accepted 11 September 2014*)

Abstract−Power and desalination plants are one of the main anthropogenic sources for CO_2 generation, which is one of the key elements to cause greenhouse gas effect and thus contribute to the global warming. Fly ash (FA) generated in desalination and power plants was converted into activated carbon (AC) treated with KOH at higher temperature and tested for CO_2 capturing efficiency. Morphological characteristics of FA such as BET specific surface area (SSA), pore volume, pore diameter, and pore size distribution (PSD) were performed using N_2 adsorption isotherm. CO_2 adsorption capacity and adsorption isotherms of CO_2 over AC were measured by performing thermogravimetric analysis at different temperatures. BET SSA of 161 m^2g^{-1} and adsorption capacity of 26 mg CO_2/g AC can be obtained by activation at KOH/FA ratio of 5 at 700 °C and activation time of 2 h. Therefore, great potential exists for producing AC from FA, which will have the positive effect of reducing the landfill problem and global warming.

Keywords: Fly Ash, Activated Carbon, CO_2 Capture, KOH Activation, Global Warming

INTRODUCTION

Global warming is attributed mainly to the increase of CO_2 emission to the atmosphere, and subsequently worst climate changes are predicted if CO_2 emission is not reduced immediately [1]. Power generation plants and seawater desalination units utilizing various fossil fuels are considered as a major contributors to this continually increasing CO_2 emission problem. This environmental problem is further aggravated by fly ash (FA) generated in these plants as a solid waste residue, which creates not only a solid waste disposal problem, but also a particulate pollution problem in the atmosphere and in the surrounding land area. The FA is being captured from flue-gas of these industries using suitable particulate collector. Currently, disposal of larger quantity of this solid waste, generated in industries, is being done in landfills, mostly without pretreatment. This has created an increasing environmental concern regarding possible leaching of heavy metals present in the FA into ground water adjacent to FA dumping sites, in addition to dusting problems [2-6].

Various utilization of FA has been implemented, tested or proposed in literature. Strength developments for cement mortars containing FA are modified by altering physical, mineralogical, morphological, and chemical properties by mechanical grinding [7-9]. FA particles and precipitated silica are used in fillers to improve the vulcanization properties of rubbers [10]. Effects of silica and alumina contents vary the setting, phase development, and physical properties of FA [11]. Nonetheless, FA whether treated or untreated, is considered as a solid waste that creates a serious pollution problem in these plants, its surroundings, and in its landfill areas. Researchers have been investigating utilization of FA with two-fold applicability, i.e., reduction of solid waste generation and handling problem and use FA generated AC to capture CO_2 emitted from these industries [12-14].

There are mainly two different processes for preparation of AC, chemical and physical activation [15-17]. An important advantage of chemical activation is its ability to take place at lower temperatures and shorter time than those used in physical activation. In addition, higher surface area and higher yield of carbon can be obtained by using chemical activation [18-20]. Many researchers have shown that AC produced by KOH activation from carbonaceous materials such as coke, charcoal, coal, and char provides a high BET SSA of over 2,000 m^2g^{-1}. In addition, KOH chemical activation is a very effective method for the production of AC with a narrow PSD and a well-developed porosity [21-26].

The aim of the present work was to investigate FA generated AC by KOH produced in power and desalination plants for removal of CO_2.

EXPERIMENTAL

1. Raw Material

The FA used for this study was obtained from Shuaiba desalination plants, 70 km south of Jeddah, Saudi Arabia. The fuel used in the desalination plant was heavy vacuum gas oil (Bunker "C"). Burning this type of fuel emits enormous amounts of obnoxious and toxic pollutants to the environment along with a large amount of a high carbon (92%) content FA (36 tons per day) [4]. The properties of raw FA generated from desalination plant are shown in Table 1.

2. Activation and Purification

About 10 g of as-received FA was mixed vigorously with 0.16 M

†To whom correspondence should be addressed.
E-mail: rathersami@gmail.com, yhamed@kau.edu.sa

Table 1. Properties of raw FA emitted from Shuaiba desalination plant in Jeddah Saud Arabia

Average particle size (μm)	Carfbon content (wt%)	Petroleum ether soluble (wt%)	Loss on ignition (LOI) (%)	Moisture content (wt%)	BET specific surface area (SSA) ($m^2\ g^{-1}$)	Pore volume ($cm^3\ g^{-1}$)
77	92	1.43	95	2.28	6.11	0.029

solution of KOH (1 g KOH per 100 ml of distilled water) to obtain a targeted weight ratio (R) of KOH to FA (R=0, 1, 2, 4, and 5) and mixture was kept in an oven to dry at 110 °C overnight. The FA impregnated with KOH was loaded in a cylindrical stainless steel reactor (2.54 cm×10 cm) closed at one end and provided with a removable cover at other end. A 2 mm hole drilled in the middle of the cover is to allow escape of vapors, gases, and pyrolysis products. A number of reactors placed in a muffle furnace and heated to the activation temperatures 500, 600, 700, 800, and 900 °C at a heating rate of 5 °C/min. At a prescribed activation time 1, 2, 3, and 4 h, a sample of each ratio was withdrawn from a furnace and allowed to cool naturally. Activated fly ash (AFA) was then neutralized by HCl followed by washing with distilled water. At the start of the process, AFA samples were placed in a 500 ml beaker, and a volume of 5 M HCl enough to neutralize the KOH initially present in the sample was added. The samples were left overnight at room temperature (RT). Next day, the supernatant was decanted and further washed by distilled water followed by decantation. The whole sample was transferred to the plastic open cone fitted with filter paper at the bottom. Sample washing continued until pH reached 6.5-7.5. After drying AFA at 110 °C overnight in a vacuum oven, its weight was determined to calculate the yield as a percentage of initial raw FA used and hereinafter referred to as the 'AC' or 'AFA'. AC samples were kept in tightly closed labeled plastic bottles placed in the desiccator.

3. Characterization

BET SSA, micropore volumes (V_{mic}), mespopore volumes (V_{mes}), and PSD of all samples of AFA were determined from nitrogen adsorption at 196 °C. A Nova 2200e instrument (Quantachrome Instruments, USA) along with a NOVAWin2 (Quantachrome Instruments) data analysis software was used for these measurements. The total pore volume (V_t) was determined from the amount of N_2 adsorbed at a relative pressure of 0.95. The NOVAWin2 software was used to perform PSD analysis by fitting the nitrogen adsorption data using density function theory (DFT) calculations assuming a slit shaped pore model [27]. Scanning electron microscopy (SEM) was used for investigating the morphological properties of the AFA.

Carbon dioxide (CO_2) adsorption capacity studies of AC were performed using a thermogravimetric analysis (TGA) apparatus (NETZSCH-Gerätebau GmbH, TG 209 F3). Analysis of TGA data was performed using NETZSCH Proteus-Thermal analysis software. About 15 to 20 mg of AC sample was used in a typical CO_2 adsorption experiment study. Prior to each adsorption experiment, a sample was placed in an alumina crucible loaded in TGA furnace and heated to 150 °C (10 °C/min.) in a flowing nitrogen (100 ml/min.) and kept at that temperature until a constant weight was obtained. This step continued for 60 to 90 minutes to ensure that surface of the AC had been properly cleaned prior commencing the adsorption measurements. After the sample was cooled to 40 °C, a gas mixture of 92% CO_2-8% N_2 (100 ml/min.) was vented into the apparatus containing AC sample at a constant temperature. The increase in sample weight was observed due to adsorption of CO_2 and maintained until the equilibrium was established. Under these conditions, adsorption capacity of CO_2 on AC was determined as the amount of CO_2 adsorbed in milligrams per gram of AC (mg CO_2/g AC). Adsorption isotherm data at different temperatures were collected in a similar manner using helium as an inert carrier to avoid effect of co-adsorption of nitrogen especially at low concentrations of CO_2.

The above-mentioned TGA and derivative thermogravimetric analysis (DTG) unit was also used to study the effects of KOH on the pyrolysis process of FA. Samples of FA loaded with different ratio's of KOH were subjected to TGA in flowing helium (100 ml/min) at a heating rate of 10 °C/min from 30 to 900 °C.

RESULTS AND DISCUSSION

1. Yield and Purity Assessment with TGA

Effects of KOH on the activation of FA were investigated using TGA and DTG, as shown in Fig. 1(a) and (b). The results of DTG

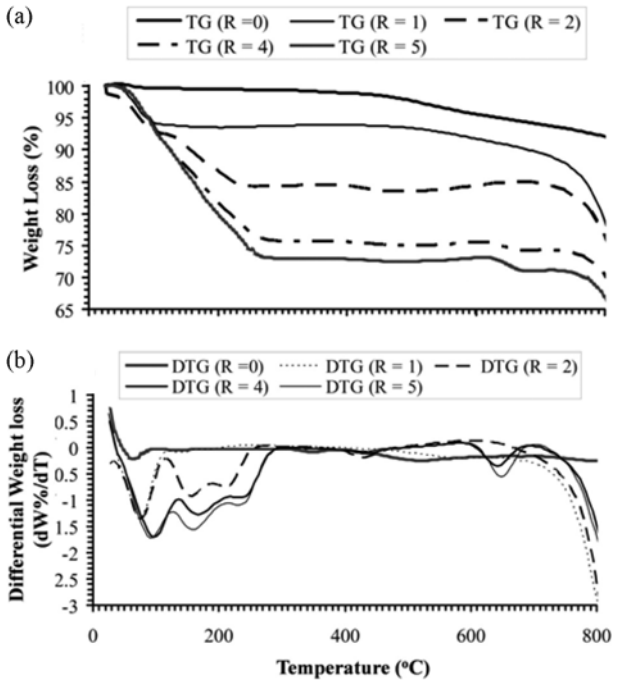

Fig. 1. TGA and DTG profiles of FA impregnated with KOH to obtain a targeted ratio of KOH/FA (R), where R is 0, 1, 2, 4, and 5 performed in He atmosphere at a ramp rate of 10 °C/min.

shown in Fig. 1(b) indicate that there are three peaks generated within the region from 80 to 250 °C. Both peak intensity and shift in temperature was observed as the ratio of KOH to FA (R) increased. Increase in peak intensity with increasing R indicates a higher rate of weight loss that can be ascribed to the fact that increasing concentration of KOH will certainly increase the rate of reaction displayed in Fig. 1(a). The main reactions considered in this region are described as follows [28]:

$$2KOH \rightarrow K_2O + H_2O \quad (1)$$

$$C + H_2O \rightarrow H_2 + CO \quad (2)$$

$$CO + H_2O \rightarrow H_2 + CO_2 \quad (3)$$

The shift in peak temperature by increasing the R is attributed to the exothermic nature of the above reactions, which will increase the system temperature. Within the temperature range from 250 to 680 °C, possible reaction is the formation of K_2CO_3 according to the reaction below:

$$K_2O + CO_2 \rightarrow K_2CO_3 \quad (4)$$

The peak generated at higher temperature (680 °C) can be attributed to the possible reactions below [29]:

$$K_2O + H_2 \rightarrow 2K + H_2O \quad (5)$$

Or

$$K_2O + CO_2 \rightarrow 2K + CO + O_2 \quad (6)$$

It is clear that generated peaks are mainly for R ratios of 4 and 5, which can be explained by the presence of residual unreacted K_2O at higher concentrations of KOH at these ratios.

2. Structural Analysis

Effects of KOH on the surface characteristics of FA produced AC were also investigated for different R ranging from 0 to 5 at a temperature 700 °C for 2 h. It is quite clear from Fig. 2 that a bimodal PSD is exhibited by the KOH impregnated FA (excluding R=0), one peak has it maxima in micropore region and the other is in the mesopore region. Similar kinds of results were also found by Rouquerol et al. [30]. The peak intensity was increased by increasing the R for both micropore and mesopore region. The above results can be ascribed to the fact that increasing available amount of KOH will increase possibility of chemical reactions between carbon and KOH, which will generate pores and slits at different locations of the treated FA. Results generated from Fig. 2 show that increasing R would increase the pore volume per unit pore diameter by a factor of 12.75 by changing the ratio from 2 to 5. In micropore region, we determined the PSD using the N_2 DFT calculations with the help of Quantachrome software [31]. FA impregnated with higher amount of KOH showed a sharp peak below ≈1 nm compared to lower amount of KOH suggesting formation of more slit shaped micropore region as compared to mesopore also confirmed by Fig. 2.

Pore size of AFA decreased with increasing R up to 4 and corresponded within the mesopore region. BET SSA increased from 13.2 to 161.3 $m^2 g^{-1}$ by increasing the ratio from 2 to 5 respectively, as shown in Fig. 3 and Table 2. BET SSA of FA without treatment of KOH merely shows 6.1 $m^2 g^{-1}$ and tremendous enhancement is observed when treated with different ratios of R. This increase in BET SSA indicates decrease in the pore diameter and creation of

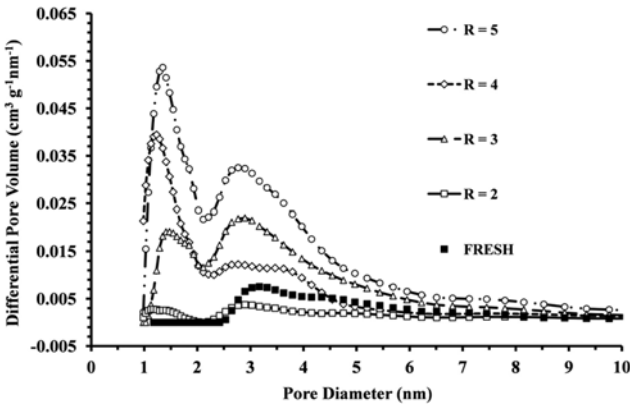

Fig. 2. Comparison of PSD by DFT of FA activated for 2 h at 700 °C and different KOH to FA ratio's.

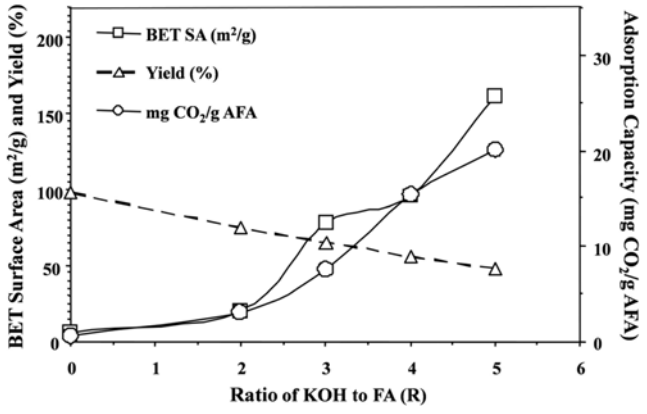

Fig. 3. Effect of ratio of KOH to fly ash (R) activated at 700 °C for 2 h on BET SSA, yield, and CO_2 adsorption capacity.

Table 2. Yield, BET SSA, and CO_2 adsorption capacity of ratio of KOH to FA (R) activated at 700 °C for 2 h

R	Yield (%)	BET SSA ($m^2 g^{-1}$)	D_p (max)	D_p (nm)	V_g ($cm^3 g^{-1}$)	V of CO_2 ads. (ml)	V of CO_2 ads. adsorb/V_T	V of CO_2 Ads./V_p<2 nm	mg CO_2/g AC
0		6.1			0	0.001			1.1
2	75	13.2	1.1	2.897	0.023	0.0028	0.1249	0.1578	3.0
3	65	78.2	1.4	2.769	0.084	0.0071	0.0855	0.5023	7.5
4	56	95.9	1.1	1.178	0.077	0.0147	0.1915	0.5034	15.4
5	48	161.3	1.3	1.348	0.148	0.0192	0.1300	0.4765	20.1

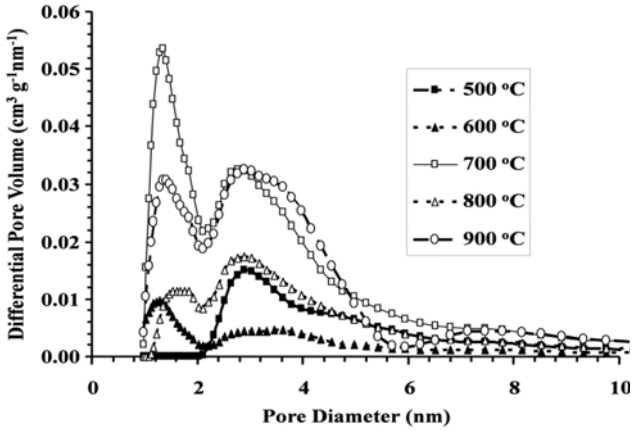

Fig. 4. Comparison of PSD by DFT of FA activated at different temperatures for 2 h and KOH to FA ratio=5.

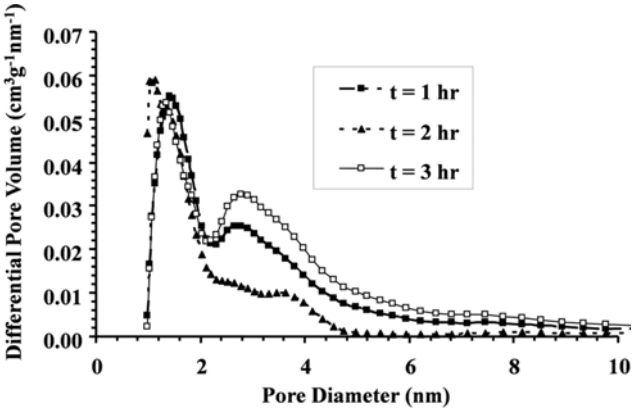

Fig. 5. Comparison of PSD of FA activated for different times at 700 °C and KOH to FA ratio=5.

defects on the surface. The amount of CO_2 adsorbed/g AC has been increased by increasing the R, as more surface area is available to accommodate higher amount of CO_2. Linear scaling of CO_2 adsorption capacity is observed in BET SSA as displayed in Fig. 3. As the KOH impregnation with FA increased, yield decreased from 75% to 48%. Formation of potassium carbonate according to Eq. (4) is expected to form at higher temperature. Further decomposition with increasing activation temperature, residence time (Fig. 6), and higher amount of R would have caused a decrease in yield. Similar kinds of results were also observed by Agullo et al. [32].

Five different activation temperatures ranging from 500 to 900 °C were investigated to find its effect on the characteristics of generated AFA as shown in Fig. 4. Pore volume per unit pore diameter increased with increasing temperature up to 700 °C, and a decrease in generated pore volume was observed as the temperatures further increased above 700 °C. Increasing the temperature above a certain limit can rupture the carbon structure to generate smaller particles, which breaks the pores and generates slit areas in the form of channels built on the surface of the generated AFA. In addition, the results displayed in Fig. 4 show that for temperatures below 700 °C, PSD is within the mesopore size range. Furthermore, it is clear for temperature at 500 °C, approximately no micropores were generated and a single peak of the mesopore size was found at ~3 nm. At temperatures (600 and 700 °C), two peaks were generated, one for micropore range and another for mesopore range. The micropore volume increases at higher activation temperature (700 °C). For higher temperatures (800 and 900 °C), a lower peak height within the micropore range was obtained, which could be due to the surface rupture at higher temperatures and generation of slits with channel shape.

Three different calcination time durations at 700 °C and KOH to FA ratio at 5 were investigated for its effect on the surface characteristics of the FA, as shown in Fig. 5. The results showed that for 2 h of activation, FA generated the highest peak intensity of micropore 1.5 nm size. It has to be clarified that increasing time duration of activation above a certain limit generates higher peak of the mesopore size range, which may be attributed to the fact that increasing activation time will certainly increase the possibility of carbon particle rupture. Furthermore, new pores with higher pore diameter are formed due to the collapse of micropores into mesopores. In addition, the slit area may be generated due to higher activation time [33]. The amount of CO_2 adsorbed/g AC has been increased by increasing the activation time, which can be ascribed to the increased BET SSA and micropore volume (V_g) due to the high acti-

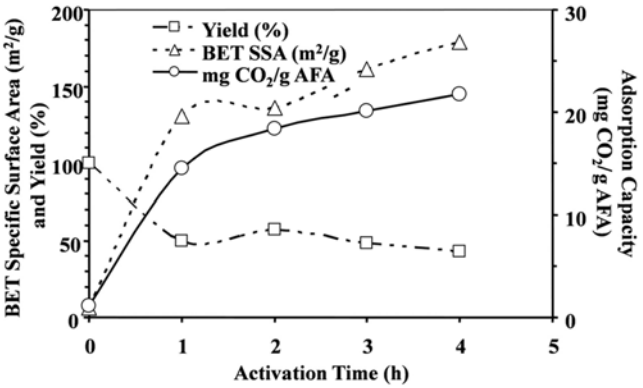

Fig. 6. Effect of activation time on BET SSA, yield, and CO_2 adsorption capacity of FA activated at 700 °C using KOH to FA ratio =5.

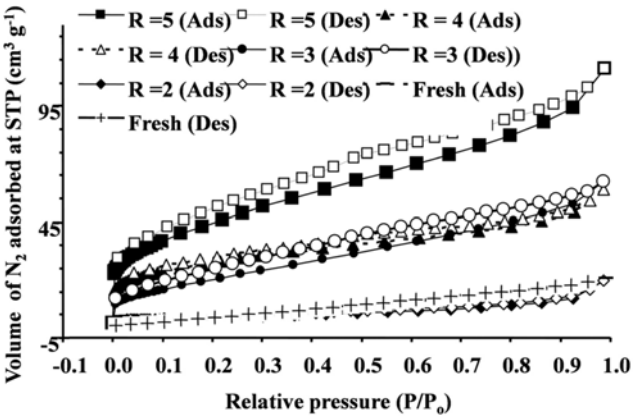

Fig. 7. Nitrogen adsorption-desorption isotherms of FA activated for 2 h at 700 °C and different ratios (KOH/FA).

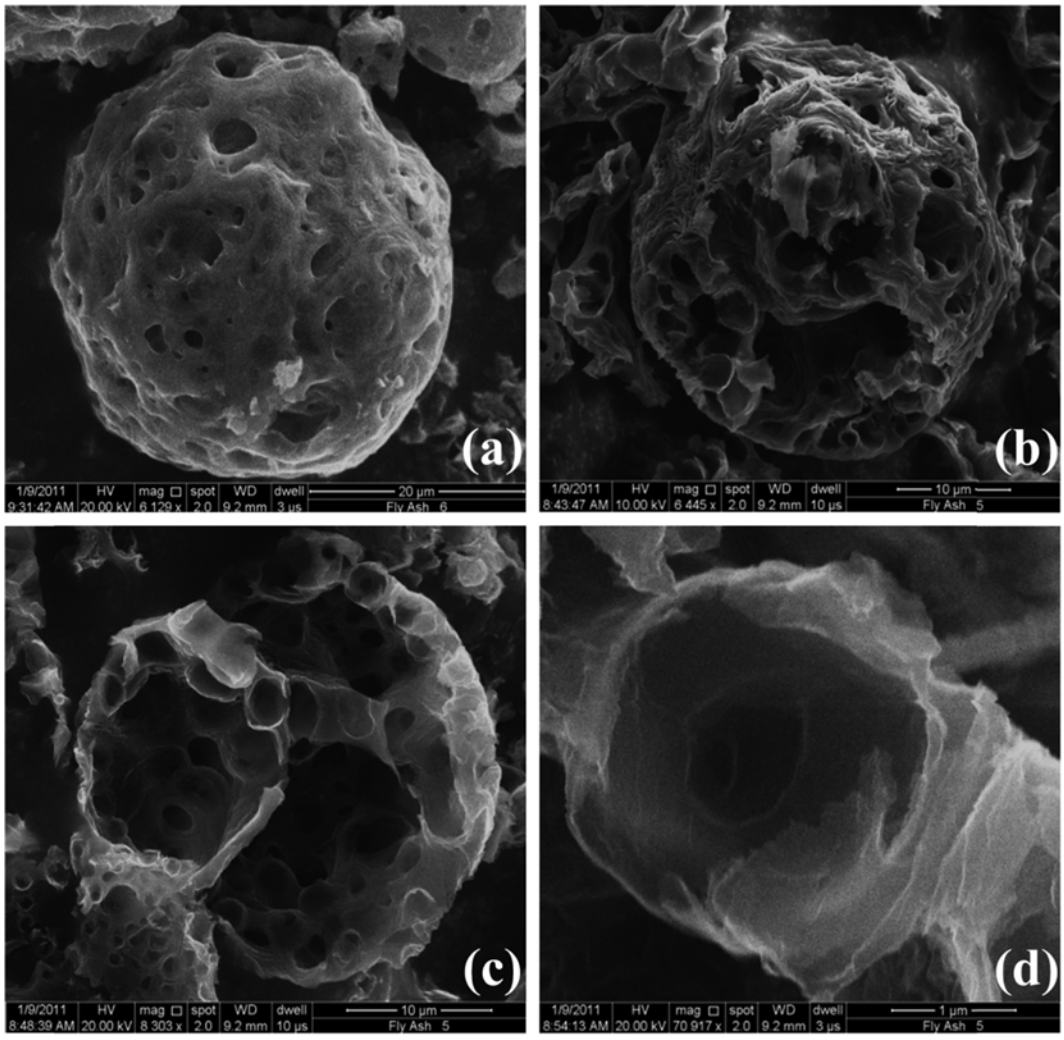

Fig. 8. SEM images of (a) fresh and (b), (c), & (d) FA treated with R=5 at a temperature of 700 °C for 2 h with different magnification.

vation time shown in Fig. 6 and Table 2.

The nitrogen adsorption-desorption isotherms of KOH/FA samples activated for 2 h at 700 °C were performed by keeping the samples isothermal at 77 K displayed in Fig. 7. According to the IUPAC classification, both nitrogen adsorption and desorption isotherms of AC can be described as a type II for samples treated with R ratios higher than 3, while for ratios below 3, the isotherm is of type III [30]. The results show that the samples treated with ratios higher than 3 have structure of macroporous type, while ratios below 3 are of non-porous type. According to Brunauer's classification, it is clear that isotherms of all treated samples behave like smooth monotonic curves, which is true for higher-pressure adsorption. According to the modern classification of hysteresis loops, the loop of adsorption-desorption isotherm for samples treated with ratios above 3 is of H3 type, indicating the adsorption is not limited at higher P/P_O. This type of isotherm occurs with aggregation of plate-like particles giving rise to slit shaped pores, while samples treated with lower ratios are of H4 type, which is nearly horizontal and parallel over a wide range of P/P_O [30,34]. The BET SSA of different R ratios (0 to 5) was estimated from the linear fit to the BET adsorption isotherms. They are found to be 6.1, 13.2, 78.2, 95.9, and 161.3 $m^2 g^{-1}$ shown in Table 2. The vast enhancement in BET SSA is totally expected for FA activated with KOH at higher temperatures. According to Yoon et al. [35] partial gasification and expansion of the interlayer spacing between the graphenes through simultaneous intercalation and deintercalation are ascribed to the higher BET SSA as R ratio are increased at higher temperatures.

SEM was used for investigating the morphological effect of KOH/FA ratio. The results show that treatment of fresh FA with KOH improves the surface porosity largely as displayed in Fig. 8(a)-(d). It is clear that fresh FA displayed in (a) was approximately free of pores and has a lower pore volume, also shown in Table 2. A new slits of a channel-like shape have been generated on the external surface of the FA shown in (b). It is clear that rupture of the carbon surface takes place approximately all over the surface as shown in (b) and (c); (c) and (d) show that pore size decreases gradually from outer surface down to the bottom depth of the pore.

3. CO_2 Adsorption Measurement

CO_2 adsorption isotherm of AC samples activated at 700 °C for 2 h with R=5 performed at different temperatures (25 °C, 30 °C,

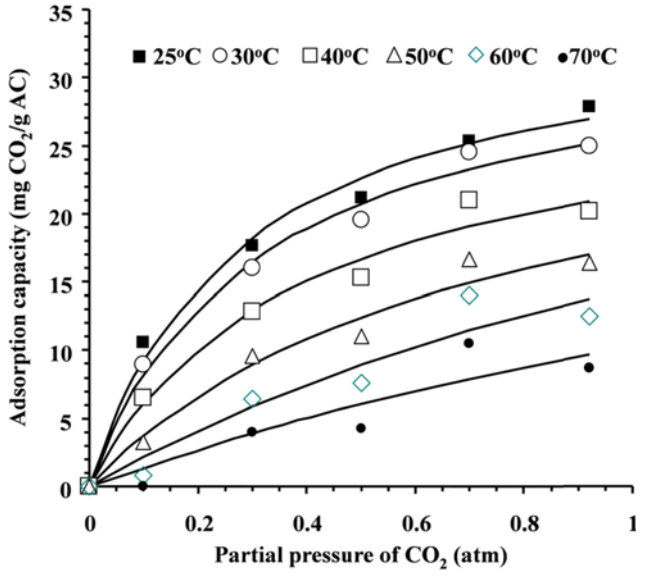

Fig. 9. Experimental (legends) and fitted Langmuir isotherm (lines) of CO_2 adsorption performed at different temperatures (25 °C, 30 °C, 40 °C, 50 °C, 60 °C, and 70 °C) on AC samples activated at 700 °C for 2 h with R=5.

40 °C, 50 °C, 60 °C, and 70 °C) and CO_2 partial pressure range 0.0 and 0.9 atm are presented in Fig. 9. For all samples, maximum CO_2 adsorption capacity linearly increases with partial pressure. Maximum CO_2 adsorption capacity of the AC sample was found to be 26 mg/g AC at 25 °C and partial pressure of 0.9 atm. CO_2 adsorption capacity of the same samples decreases as the temperature increases under similar experimental conditions. Physical adsorption is an exothermic reaction feasible at lower temperature and decreases as the temperature increases follows Le Chatelier's principle. FA generated AC having highest BET SSA (161.3 $m^2 g^{-1}$) shows maximum CO_2 adsorption capacity (20.1 mg/g AC) at 40 °C as displayed in Table 2 and Fig. 9. Linear scaling of CO_2 adsorption capacity with BET SSA is shown in Fig. 10. CO_2 adsorption data obtained at different temperatures were fitted to Langmuir isotherm to esti-

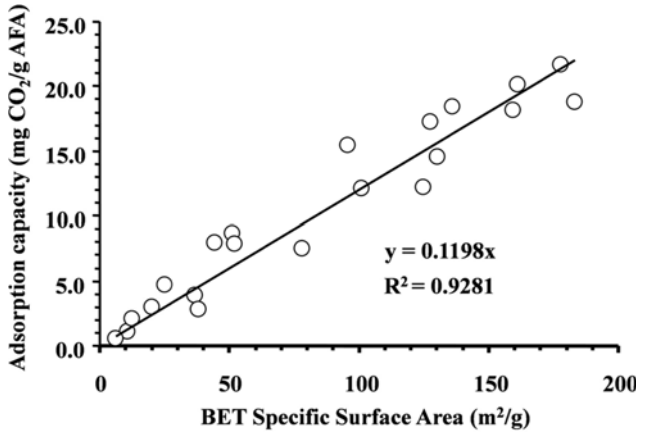

Fig. 10. The linear scaling of adsorption capacity of CO_2 (92% CO_2 in N_2 at 40 °C) of AC with BET SSA.

Table 3. Effect of temperature on K and q_m of AC samples activated at 700 °C for 2 h with R=5

Temperature (K)	298	303	313	323	333	343
q_m (mg CO_2/g AC)	35.2	33.75	29.17	30.46	38.72	35.2
K	3.57	3.17	2.55	1.38	0.6	0.41
R^2	0.991	0.992	0.981	0.974	0.929	0.84

mate the maximum adsorption capacity (monolayer coverage), q_m and the adsorption equilibrium constant (K) according to the Langmuir equation [34]:

$$q_e = q_m \frac{Kp_e}{1+Kp_e} \tag{7}$$

where p_e is the equilibrium partial pressure of CO_2. Nonlinear regression software (Polymath) was used to determine Langmuir equation parameters (q_m, and K) and R^2 (correlation coefficient) as a statistical indicator of goodness of model prediction. It is customary to conclude that R^2 close to unity indicates that model represents the data accurately. Langmuir isotherms accurately describe the CO_2 adsorption data on AC with R^2 values in excess of 0.929 for most of the temperatures as shown in Fig. 9 and Table 3. The value of q_m varies within a narrow range with a mean value of 33.75± 3.48 mg CO_2/g AC as the temperature increases from 25 °C to 70 °C. Thus, it is plausible to assume that q_m does not change significantly within the temperature range investigated.

From thermodynamic principles, it is known for a chemical system at equilibrium [36]:

$$\Delta G = -RT \ln K \tag{8}$$

where ΔG, R, T, and K is Gibbs free energy, universal gas constant, absolute temperature, and equilibrium constant. Also

$$\Delta G = \Delta H - T\Delta S \tag{9}$$

where ΔH and ΔS is the heat of reaction and entropy change. From Eqs. (8) and (9), it can be shown that

$$\ln K = \frac{\Delta S}{R} - \frac{\Delta H}{RT} \tag{10}$$

On the other hand, according to Langmuir single site adsorption mechanism, we can write the reversible adsorption reaction:

$$A + S = A.S$$

where A and S is an adsorbate and adsorption site. The Arrhenius form of adsorption and desorption rate constants can be written as follows:

$$k_{ads} = A_{ads} e^{\frac{-E_{ads}}{RT}} \tag{11}$$

$$k_{des} = A_{des} e^{\frac{-E_{des}}{RT}} \tag{12}$$

where A_{ads}, A_{des}, E_{ads}, E_{des}, k_{ads}, and k_{des} are adsorption frequency factor, desorption frequency factor, adsorption activation energy, desorption activation energy, adsorption rate constant, and desorption rate constant, respectively. From Eqs. (11) and (12), it can be shown that

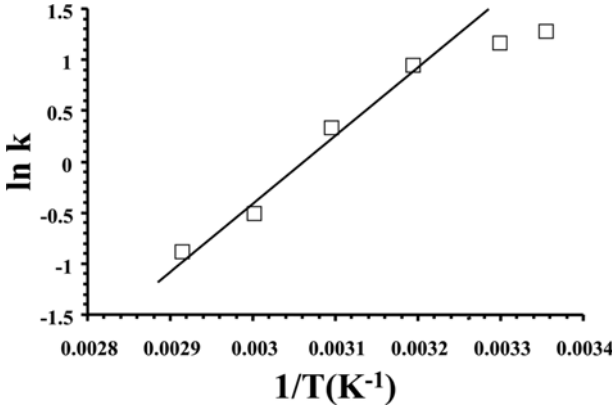

Fig. 11. Relationship between ln K and 1/T of AC samples activated at 700 °C for 2 h with R=5.

Table 4. Effect of temperature range on (E_{des}–E_{ads}) of AC samples activated at 700 °C for 2 h with R=5

Temperature range (K)	(A_{ads}/A_{des})	($E_{des}-E_{ads}$) kcal/mol	R^2
298-313	3.227×10^{-3}	4.13	0.9999
313-343	9.572×10^{-10}	13.45	0.9858

$$\ln K = \frac{E_{des}-E_{ads}}{RT} + \ln\frac{A_{ads}}{A_{des}} \quad (13)$$

Comparing Eqs. (10) and (13), it is clear that

$$E_{ads}-E_{des}=\Delta H \quad (14)$$

$$\ln\frac{A_{ads}}{A_{des}}=\frac{\Delta S}{R} \quad (15)$$

Thus, the heat of adsorption can be calculated from plotting ln K versus 1/T as shown in Fig. 11. It is clear that there are two regions, one at lower temperatures (25 to 40 °C) with lower heat of adsorption (ΔH=4.13 kcal $mole^{-1}$) and other is at higher temperature range (40 to 70 °C) with higher heat of adsorption (13.45 kcal mol^{-1}), as shown in Table 4. According to Yang et al. [37] the heat of physical adsorption is below 10-15 kcal mol^{-1}. According to this criterion, lower activation energy obtained between 25 to 40 °C certainly indicates physical adsorption nature of CO_2 on AC. However, increase of heat of adsorption to 13.45 kcal mol^{-1} for high temperature range (40 to 70 °C), although could be considered as physical adsorption. It may also indicate a change in the nature of adsorption of CO_2 at higher temperature.

CONCLUSION

A reasonably high BET specific surface area (SSA) activated carbon (AC) was successfully prepared by treating the desalination and power plant generated fly ash (FA) with KOH. The highest BET SSA for the AC was found to be 161 m^2/g AC by optimizing the process conditions such as FA to KOH ratio 5, calcination duration for 2 h, and activation temperature at 700 °C. Adsorption isotherms were generated for CO_2 adsorption on this optimized AC and maximum adsorption capacity was found about ~26 mg CO_2/g AC at 40 °C. Investigations also revealed that even though CO_2 absorption on AC is not very high, but it opens a new kind of research, where CO_2 emitted from desalination and power plants can be adsorbed back on the same FA generated within the same plant. Curtailing CO_2 emitted from the above sources suggests modest reduction of greenhouse gas emission, which in turn will help to reduce global warming. In future, modification of FA post generation from power and desalination plants to obtain a very high BET SSA can accommodate more CO_2 may help to reduce greenhouse gas emission to a greater extent.

ACKNOWLEDGEMENT

Funding for this research project (1/H/1) was provided by the Center of Excellence in Environmental Studies, King Abdulaziz University.

REFERENCES

1. M. M. M. Valer, C. Song and Y. Soong, *Environmental challenges and greenhouse gas Control for fossil fuel utilization in the 21st Century,* Springer (2003).
2. C. L. Quere, *Earth Syst. Sci. Data*, **6**, 689 (2013).
3. M. Daous, *The 20th International conference on solid waste technology and management,* Philadelphia, USA (2005).
4. M. M. Rahman, A. G. Dalvi, K. A. Rabbani, S. Al-Sulami, F. Mandili, H. M. Khaledi and B. Al-Jowdi, *Evaluation of fuel chemical additives to reduce corrosion and stack emission in SWCC power plants, 4th SWCC Acquired Experience Symposium*, Jeddah, Saudi Arabia (2005).
5. S. Wang and H. Wu, *J. Hazard. Mater.* B, **136**, 482 (2006).
6. D. C. Adriano, A. L. Page, A. A. Elseewi, A. C. Chang and I. Straughan, *J. Environ. Qual.*, **9**, 333 (1980).
7. J. Paya, J. Monzo, M. V. Borrachero, E. Peris and E. G. Lopez, *Cem. Concr. Res.*, **27**, 1365 (1997).
8. K. D. Weerdt, M. B. Haha, G. L. Saout, K. O. Kjellsen, H. Justnes and B. Lothenbach. *Cem. Concr. Res.*, **41**, 279 (2011).
9. R. J. Flatt, N. Roussel and C. R. Cheeseman, *J. Eurp. Ceram. Soc.*, **32**, 2787 (2012).
10. N. Sombatsompop, S. Thongsang, T. Markpin and E. Wimolmala, *J. Appl. Polym. Sci.*, **93**, 2119 (2004).
11. P. Chindaprasirt, P. D. Silva, K. Sagoe-Crentsil and S. Hanjitsuwan, *J. Mater. Sci.*, **47**, 4876 (2012).
12. D. P. Vargas, L. Giraldo and J. C. M. Piraján, *Int. J. Mol. Sci.*, **13**, 8388 (2012).
13. D. M. D. Alessandro, B. Smit and J. R. Long, *Angew. Chem. Int. Ed.*, **49**, 6058 (2010).
14. C. H. Yu, C. H. Huang and C. S. Tan, *Aerosol Air Qual. Res.*, **12**, 745 (2012).
15. R. C. Bansal, J. B. Donnet, F. Stoeckli and M. Deckker, *J. Dispersion Sci. Technol.*, **11**, 323 (1990).
16. M. Valix, W. H. Cheung and G. McKay, *Chemosphere*, **56**, 493 (2004).
17. T. H. Usmani, M. Tahir, I. Siddiqui and F. A. Parveen, *J. Chem. Soc. Pak.*, **25**, 183 (2003).

18. F. Caturla, M. M. Sabio and F. R. Reinoso, *Carbon*, **29**, 999 (1991).
19. A. A. Pour and D. D. Do, *Carbon*, **34**, 471 (1996).
20. K. Somna, C. Jaturapitakkul, P. Kajitvichyanukul and P. Chindaprasirt, *Fuel*, **90**, 2118 (2011).
21. F. C. Wu, P. H. Wu, R. L. Tseng and R. S. Juang, *J. Environ. Manage.*, **91**, 1097 (2010).
22. R. L. Tseng, S. K. Tseng, F. C. Wu, C. C. Hu and C. C. Wang, *J. Chin. Inst. Chem. Eng.*, **39**, 37 (2008).
23. M. A. L. Rodenas, J. J. Juan, D. C. Amoros and A. L. Solano, *Carbon*, **42**, 1371 (2004).
24. M. A. L. Rodenas, D. C. Amoros and A. L. Solano, *Carbon*, **41**, 267 (2003).
25. G. G. Stavropoulos, *Fuel Process. Technol.*, **86**, 1165 (2005).
26. L. Chunlan, X. Shaoping, G. Yixiong, L. Shuqin and L. Changhou, *Carbon*, **43**, 2295 (2005).
27. S. Lowell, J. E. Shields, M. A. Thomas and M. Thommes, *Characterization of Porous Solids and Powders: Surface Area, Pore Size and Density*, Kluwer Academic Publishers, Netherland (2004).
28. T. Yang and A. C. Lua, *J. Colloid Interface Sci.*, **267**, 408 (2003).
29. M. J. I. Gómez, A. G. García, C. S. M. de Lecea and A. L. Solano, *Energy Fuels*, **10**, 1108 (1996).
30. F. Rouquerol, J. Rouquerol and K. Sing, *Adsorption by powders and porous solids: Principles methodology and applications*, Academic Press, London (1999).
31. G. Horvath and K. Kawazoe, *J. Chem. Eng. Jpn.*, **16**, 470 (1983).
32. J. A. M. Agullo, B. C. Moore, D. C. Amoros and A. L. Solano, *Micropor. Mesopor. Mater.*, **101**, 397 (2007).
33. Allwar, A. M. Noor and M. A. M. Nawi, *J. Phys. Sci.*, **19**(2), 93 (2008).
34. G. Aranovich and M. Donohue, *J. Colloid Interface Sci.*, **194**, 392 (1997).
35. S. H. Yoon, S. Lim, Y. Song, Y. Ota, W. Qiao, A. Tanaka and I. Mochida, *Carbon*, **42**, 1723 (2004).
36. F. Rouquerol, J. Rouquerol and K. Sing, *Adsorption by Powders and Porous Solids: Principles, Methodology and Applications, First edition*, Academic Press (1998).
37. R. T. Yang, *Gas separation by adsorption process, vol. 1*, Imperial College Press, Boston (1997).